Successive Dynamical Steps of Photoinduced Switching of a Molecular Fe(III) Spin-Crossover Material by Time-Resolved X-Ray Diffraction

M. Lorenc,[1] J. Hébert,[1] N. Moisan,[1] E. Trzop,[1] M. Servol,[1] M. Buron-Le Cointe,[1,2] H. Cailleau,[1,2] M. L. Boillot,[3] E. Pontecorvo,[4] M. Wulff,[4] S. Koshihara,[5] and E. Collet[1,2,*]

[1]*Institut de Physique de Rennes, Université de Rennes 1-CNRS, UMR 6251, 35042 Rennes, France*
[2]*ERATO, Japan Science and Technology Agency, 3-5 Sanbanchou, Chiyoda-ku, Tokyo 102-0075, Japan*
[3]*Institut de Chimie Moléculaire et Matériaux d'Orsay, UMR-CNRS 8182, Université Paris-Sud, 91405 Orsay, France*
[4]*European Synchrotron Radiation Facility, 38043 Grenoble, France*
[5]*Tokyo Institute of Technology, 2-12-1 Oh-okayama, Meguro-ku, Tokyo 152-8551, Japan*
(Received 25 July 2008; published 10 July 2009)

We investigate the out-of-equilibrium switching dynamics of a molecular Fe(III) spin-crossover solid triggered by a femtosecond laser flash. The time-resolved x-ray diffraction and optical results show that the dynamics span from subpicosecond local photoswitching followed by volume expansion (nanosecond) and thermal switching (microsecond). We present a physical picture of the consecutive steps in the photoswitching of molecular materials.

DOI: 10.1103/PhysRevLett.103.028301 PACS numbers: 82.53.Xa, 61.50.Ks, 78.47.Fg, 78.47.jc

New opportunities appear for light control of various functionalities of materials (magnetic, optical, conduction...), especially through the macroscopic switching of physical properties induced by ultrashort laser pulses [1–3]. Materials with photoactive multifunctional molecules are particularly promising to explore. Among these, spin-crossover compounds [4] are prototypes of molecular bistability in the solid state. The molecules (Fig. 1) may be switched from low-spin (LS) to high-spin (HS) states under various external perturbations, including light irradiation [4]. This switching leads to a change in magnetic and optical properties as well as a structural reorganization, including a change in the volume of the unit cell. The design of bistable spin-crossover films [5] and nanoparticles [6,7], as well as the observation of bidirectional photoswitching inside thermal hysteresis [8,9], represent important progress toward molecular memory devices. In spite of these progresses, the pertinent time scales for photoswitching processes in these materials are still unknown, since previous investigations dealt mainly with the kinetics of recovery to the thermally stable state [10,11]. In solids, we can expect the dynamics to follow a complex pathway from molecular to material scale through a sequence of processes. Time-resolved diffraction [12–17] is a direct method to probe the real time structural dynamics of matter, such as a change of molecular geometry, unit-cell volume and thermal motions. Structural investigations of light-driven switching of spin-crossover solids have so far been limited to photo-stationary states at low temperature [18,19]. By combining time-resolved optical and x-ray diffraction techniques, we demonstrate that the spin-state photoswitching dynamics triggered by a femtosecond (fs) laser is a multistep out-of equilibrium process. It spans from the subpicosecond (ps) local molecular photoswitching to slower volume expansion and to μs thermoswitching of the macroscopic solid.

In this study we examine the photoswitching dynamics of the monoclinic polymorph of $[(TPA)Fe(III)(TCC)]PF_6$ [20,21]. It undergoes a thermal spin crossover from a low temperature LS ($S = 1/2$) to a high temperature HS ($S = 5/2$) state [Figs. 1 and 2(a)]. The conversion is gradual, centered at $T_{1/2} \approx 214$ K where the HS population (X_{HS}) is 50%. This indicates a weakly cooperative system, by contrast to strongly cooperative ones presenting first-order phase transitions [4]. The variation of X_{HS} [20] concurrently modifies the magnetic susceptibility, the optical properties and the molecular structure mainly around the central Fe ion [Fig. 2(a) and see also Figs. S1 and S2 in the supplementary material]. The elongation of Fe-N bond length is a well-known fingerprint of increased spin multiplicity from electron transfer to less bonding orbitals. The

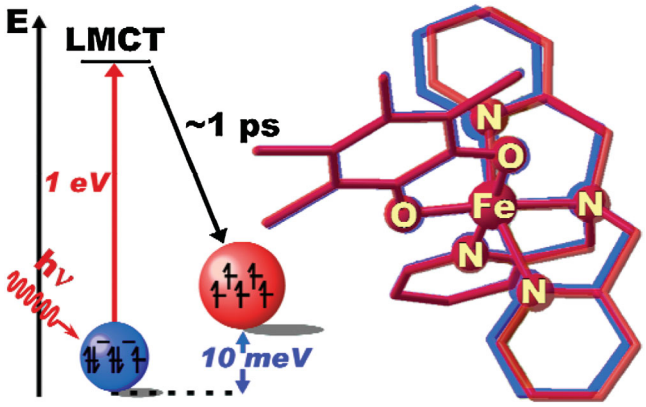

FIG. 1 (color). The spin-crossover cation $[(TPA)Fe(III)(TCC)]^+$ (PF_6^- anions are not shown for clarity), TPA denotes tris(2-pyridylmethyl) amine, TCC denotes 3,4,5,6-tetrachlorocatecholate dianion. Optical excitation path between the LS (blue) to HS (red) states schematically shown on the left and corresponding blue and red cation structures on the right.

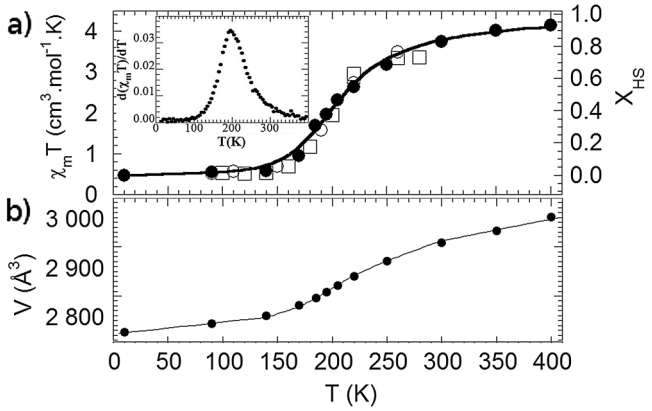

FIG. 2. (a) Temperature dependence of the magnetic response $\chi_m T$ (solid line, left axis), its derivative (inset) and of X_{HS} (right axis). The temperature variation of the optical reflectivity at 532 nm (○), the optical transmission at 600 nm (□) and the ⟨Fe-N⟩ bond length (●) were scaled to X_{HS} (right axis). (b) Temperature dependence of the unit-cell volume.

average value varies here from $\langle \text{Fe-N} \rangle_{LS} = 1.963(1)$ Å at 18 K to $\langle \text{Fe-N} \rangle_{HS} = 2.125(1)$ Å at 400 K, typical values for LS and HS states [4,22]. The thermal LS to HS conversion translates to large change of unit-cell volume around $T_{1/2}$ [Fig. 2(b)]. The temperature dependence of ⟨Fe-N⟩ being the X_{HS} and (1-X_{HS}) weighted contribution of $\langle \text{Fe-N} \rangle_{HS}$ and $\langle \text{Fe-N} \rangle_{LS}$, allows scaling ⟨Fe-N⟩ to X_{HS} [Fig. 2(a), S2] [20]. The changes of optical properties [20] [in this case transmission at 600 nm, and reflectivity at 532 nm), also scaled to X_{HS}, clearly indicates correlation between magnetic, x-ray, and optical probes [Fig. 2(a)].

The response of 15 μm thick single crystals to a 100 fs pump laser pulse at 800 nm (penetration depth 3–5 μm) was investigated by time-resolved optical experiments [20] with light polarized along the long crystal axis ***a*** and typical photon densities of up to 150 $\mu J/mm^2$ (damage threshold ≈ 300 $\mu J/mm^2$). First we captured the photogeneration of HS molecules by continuous wave (cw) optical reflectivity [scaled to HS concentration change ΔX_{HS}, Fig. 3(a)] gated electronically with 100 μs resolution. As indicated in Fig. 3(a), the response of the crystal 100 μs after photoexcitation is referred to as μs amplitude.

The ultrafast dynamics were studied with 1 kHz optical pump-probe experiment with 100 fs time-resolution down to 90 K. At lower temperatures the equilibrium recovery time becomes too long. The optical transmission following 40 $\mu J/mm^2$ excitation was measured at 600 nm and 480 nm [Fig. 3(b)] wavelengths for which transmission varies with opposite signs during the spin-crossover (Fig. S1 in [20]). A transient absorption peak due to a Ligand-to-Metal Charge-Transfer state (LMCT [23,24]), similar at both wavelengths, appears within the experimental resolution. The transmission rises at 600 nm and drops at 480 nm between negative delays and 1 ps after laser excitation. It obeys the spectral variations observed at

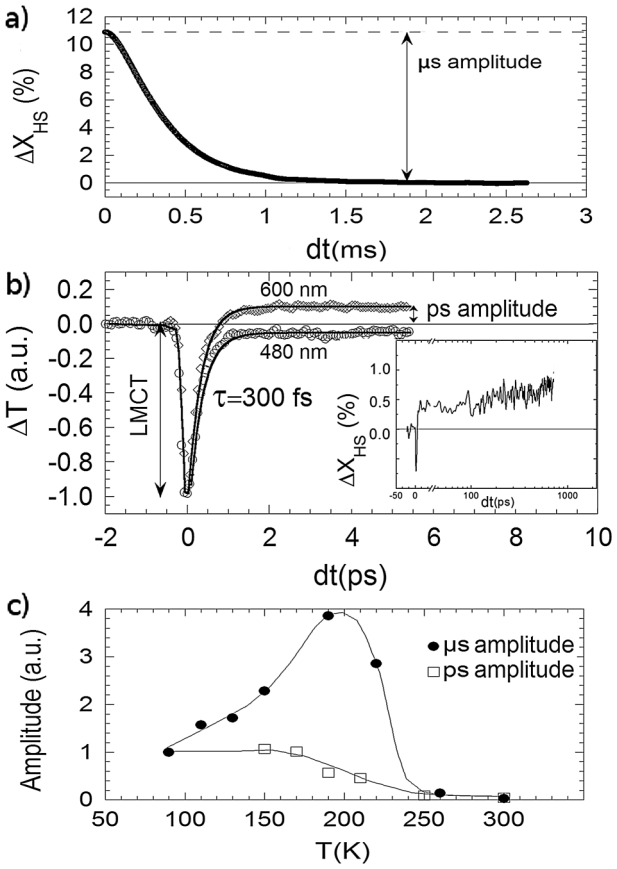

FIG. 3. Optical signatures of spin-state photoswitching. (a) Variation of the cw reflectivity at 532 nm after fs laser excitation at 190 K, scaled to X_{HS}. (b) Time dependence of the variation of transmission ΔT at 600 and 480 nm at 190 K. Evolution of X_{HS} on the ps plateau shown in the inset. (c) Temperature dependence of the μs amplitude and ps amplitude from (a) and (b) normalized to 1 at 90 K. Optical signals are converted to HS concentration change ΔX_{HS} according to correlations shown in Fig. 2(a).

thermal equilibrium (Fig. S1), leaving a clear fingerprint of HS state in nonthermal conditions. This signal which remains nearly constant on a plateau between 1 and 100 s of picoseconds is hereafter referred to as ps amplitude, as illustrated with the inset in Fig. 3(b). At 190 K, the photoconverted HS fraction on this ps plateau is $\Delta X_{HS} \approx 0.5\%$. The plateau collapses at high temperature [Fig. 3(c)] where the fraction of LS molecules is close to 0, indicating that excitation at 800 nm induces mainly a LS to HS switch.

The structural analysis [20] with 100 ps resolution was performed on the beamline ID09B (ESRF [8,10]), to directly probe the nature of the photoinduced state on the ps plateau. Simultaneous top and bottom illumination of the crystal was used to maximize the transformation rate (≈150 $\mu J/mm^2$). At 180 K the associated variation of the characteristic intramolecular bonds $\Delta\langle \text{Fe-N} \rangle$ is ≈0.005 Å on the ps plateau [Fig. 4(a)], thus providing a structural evidence of the photogeneration of HS molecular states in the early stage. $\Delta\langle \text{Fe-N} \rangle$ reaches even ≈0.01 Å on μs

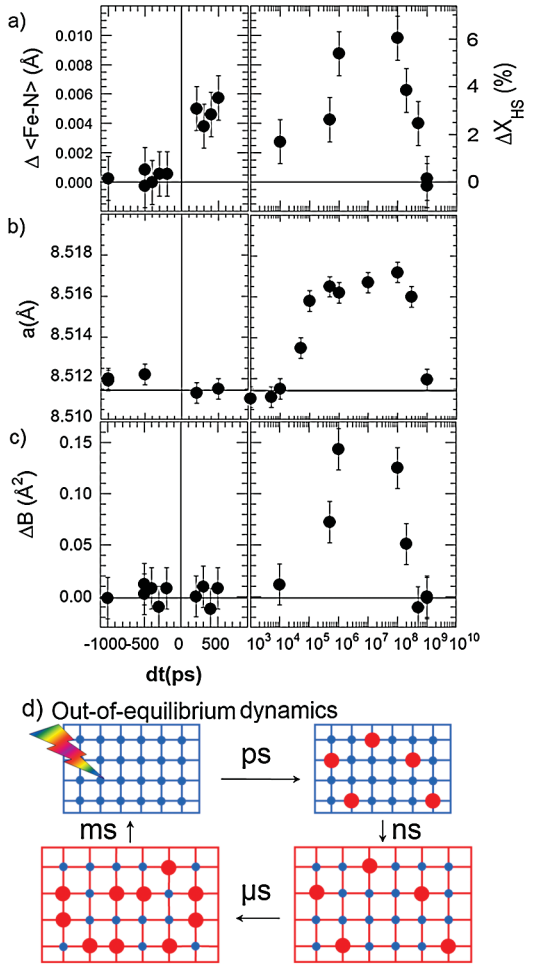

FIG. 4 (color). Time dependent structural changes at 180 K on a linear-log scale: (a) ΔX_{HS} deduced from $\Delta\langle$Fe-N$\rangle$, (b) lattice parameter a and (c) isotropic temperature factor variation ΔB. (d) Schematic drawing of the dynamics: HS molecules (red circles) generated within 1 ps by laser pulse in the cold (blue) lattice with mainly LS molecules (blue circles), warm lattice (red) expansion on 10 s ns, thermal stabilization of HS population within μs. Recovery to thermal equilibrium of the crystal with the environment (cryostat) on ms time scale. The error bars account for the experimental precision.

scale. Scaled to ΔX_{HS} [20], $\Delta\langle$Fe-N$\rangle$ reveals an instantaneous $\approx$3% rise on the ps plateau and $\approx$6% around 100 μs [Fig. 4(a)] [25]. Variations of ΔX_{HS} from optical and x-ray data compared to used excitation densities indicate that a single absorbed photon transforms a single molecule during this early stage. This first step of the photoinduced transformation is hereafter denoted (i). After a lapse of about 50 ns, a second step labeled (ii) is observed, corresponding to the lattice expansion [parameter ***a*** [20] Fig. 4(b)]. The same expansion around 50 ns was observed at 120 and 160 K. Another point to explore concern thermal effects which should set-in at some stage since energy is deposited in the crystal with the fs laser pulse. We then constructed Wilson plots to obtain an indirect measure of the temperature increase due to heating at macroscopic scale (Fig. S3). The obtained variation of the isotropic temperature factor ΔB indicates that this heating appears on μs time scale [Fig. 4(c)] which is the third step of the transformation, later denoted (iii). The recovery to thermal equilibrium with the sample environment occurs within milliseconds.

Regarding step (i) direct LS to HS transition is forbidden, as it involves a $\Delta S = 2$ change of spin [24]. While it is well established that Franck-Condon excitation proceeds through the initial population of different charge-transfer states, here referred to as LMCT [24], the subsequent relaxation pathways down to the low-lying HS state are still a matter of discussion [4,26,27]. Optical signatures [Fig. 3(b)] indicate that the HS state is populated from the LMCT state, fitted by an exponential function with 300 fs time constant. The relaxation cascade from LMCT to HS state occurs within less than one ps, which is similar to time scales reported for spin-crossover molecules in solution [23,26,27] and recently in the orthorhombic polymorph [28] of [(TPA)Fe(TCC)]PF_6. While the very first steps of LS-HS conversion elude our resolution, we provide spectroscopic evidence of its ultrafast nature, directly confirmed with x-ray showing increased $\Delta\langle$Fe-N$\rangle$. The 100 fs time scale is therefore the bottleneck for local spin-state switching.

This first stage of the transformation, corresponding to local molecular switching, manifests itself by intramolecular reorganization at constant volume. Indeed volume expansion involves propagation of cell deformation inside the crystal. Step (ii) is therefore limited by the speed of sound, as demonstrated in liquids [16] under similar experimental conditions. Given the $\approx$100 μm laser spot size and typical sound velocity (order of 1000 $\mathrm{m \cdot s^{-1}}$), the volume expands on a few tens of nanoseconds consistently with Fig. 4(b). This effect may have two origins: first the elastic interaction resulting from swelling of photo-transformed HS molecules, and second the local heating caused by nonradiative energy dissipation of relaxing LMCT states. The absorbed optical energy ($\approx$1.55 eV) is much higher than the energy difference between LS and HS states (10 s of meV [4]), in Fig. 1. Resulting increase of local temperature and pressure drives volume expansion. However, during step (ii) the photo-switched molecules are not yet at thermal equilibrium with the lattice bath as explained hereafter.

Two points are worth discussing in relation with step (iii). Firstly, the lattice expansion around 50 ns can favor the HS state but no apparent simultaneous increase of X_{HS} is observed at this stage. The HS population increase from 3 to 6% on microseconds delays is then mainly associated with a thermally activated process. This kinetics process is governed by energy barriers and the corresponding rate constants were obtained for a series of similar Fe(III) solids [10]. From there, we estimate that relative LS/HS population becomes thermally equilibrated with the lattice in a time of the order of μs. Second, heat diffusion through the 15 μm thick sample to restore temperature homogeneity

has to be taken into account. Because of the finite penetration depth ($\approx$3–5 μm), the pump laser causes gradients of deposited energy and of local temperature. The time required to homogenize temperature across the crystal is governed by heat diffusivity and typical values of the order 10^{-6} $m^2 \cdot s^{-1}$ correspond to the 10–100 μs. A significant variation of the isotropic temperature factor (ΔB) observed in Fig. 4 is a consequence of temperature homogenization. The overall temperature increase ΔT depends on the amount of energy E deposited by the laser pulse and heat capacity ($C_p \approx 250$–500 $J\,Mol^{-1}\,K^{-1}$ [4]), as $\Delta T = E/C_p$. For the laser energy used and number of moles contained in the probed volume, we expect a 7–15 K temperature rise. This fits well with the $\approx$15 K deduced from the values of ΔX_{HS} at 100 μs in Fig. 4(a) scaled to temperature change according to Fig. 2. This thermal conversion is further manifested by the temperature dependence of reflectivity on the microsecond time scale, which peaks around 200 K [Fig. 3(c)]. A temperature shift of dT induces the highest variation of X_{HS} where dX_{HS}/dT is maximal ($\approx$200 K, Fig. 2). Such behavior underlines the active role of the optically silent molecules in the bulk solid. The optical response on the ps time scale [Fig. 3(c)] is markedly different. It does not exhibit the typical maximum around $T_{1/2}$ but follows the LS concentration ($1\text{-}X_{HS}$) instead. It is yet another illustration of the fact emphasized throughout this work, that short time-scale dynamics are limited to photo-activated molecules.

The out-of-equilibrium dynamics towards the macroscopic switching, when triggered by ultrashort laser pulse, involves consecutive steps over different time scales. This situation with localized molecular photoexcitation differs from the delocalized electronic excitation discussed in the literature [12,29]. In the latter, the new potential resulting from electronic redistribution after the fs thermalization of hot electrons may lead to lattice instability. The subsequent coherent optical phonon mode softens nonthermally in a cold lattice. Processes ensuing on longer time scales, such as lattice thermalization and unit-cell deformation, remain a subject of debate. In the case of the localized molecular excitation investigated here, the first step corresponds to ''hot'' molecules dispersed in a cold solid. The existence of different steps, summarized in Fig. 4(d), reflects a sequence of physical processes: local LMCT to HS relaxation cascade with bond-length evolution for step (i), propagation of cell deformation for step (ii) and LS to HS thermal switching for step (iii). We believe that these results will stimulate theoretical work developed nowadays [30] to a deeper understanding of the response of an assembly of molecules to a local excitation. The multistep transformation process differs fundamentally from the ms exponential-like relaxation [Fig. 3(a)]. The recovery to thermal equilibrium with the sample environment is governed by thermal processes [10]. The ms time scale of this stochastic dynamics is much longer than that of more elementary physical processes (molecular and unit-cell deformations), which are therefore hidden in a statistical average. These elementary processes are only resolved during the phototransformation since they are clocked by the ultrashort laser pulse, as evidenced here with pump-probe methods. The above results shed new light on the complex switching pathway from the molecular to material length and time scales. This is important for the design of materials with enhanced functionality.

This work was supported by the Institut Universitaire de France, the Ministry of Research of France (ACI JC E. Collet, ANR NT05-3_45333), Europe (MRTN-CT-2003-503641), Région Bretagne (CREATE Ultimate 4146, PRIR Femtocom 2178, SIE MagBreiz 2142, Ph.D. funding of J. H.) and Rennes Métropole.

*To whom correspondence should be addressed.
Eric.Collet@univ-rennes1.fr

[1] M. Rini *et al.*, Nature (London) **449**, 72 (2007).
[2] M. Chollet *et al.*, Science **307**, 86 (2005).
[3] S. Koshihara and S. Adachi, J. Phys. Soc. Jpn. **75**, 011005 (2006).
[4] *Spin Crossover in Transition Metal Compounds: Topics in Current Chemistry*, edited by P. Gütlich and H. A. Goodwin (2004), p. 233.
[5] S. Cobo *et al.*, Angew. Chem., Int. Ed. **45**, 5786 (2006).
[6] E. Coronado *et al.*, Adv. Mater. **19**, 1359 (2007).
[7] T. Forestier *et al.*, Chem. Commun. (Cambridge) **37**, 4327 (2008).
[8] E. Freysz *et al.*, Chem. Phys. Lett. **394**, 318 (2004).
[9] S. Cobo *et al.*, J. Am. Chem. Soc. **130**, 9019 (2008).
[10] C. Enachescu *et al.*, Chem. Phys. Chem. **7**, 1127 (2006).
[11] O. Fouché *et al.*, Chem. Phys. Lett. **469**, 274 (2009).
[12] N. Gedik *et al.*, Science **316**, 425 (2007).
[13] A. Cavalleri *et al.*, Nature (London) **442**, 664 (2006).
[14] E. Collet *et al.*, Science **300**, 612 (2003).
[15] A. Rousse *et al.*, Nature (London) **410**, 65 (2001).
[16] M. Wulff *et al.*, J. Chem. Phys. **124**, 034501 (2006).
[17] S. Nozawa *et al.*, J. Synchrotron Radiat. **14**, 313 (2007).
[18] N. Huby *et al.*, Phys. Rev. B **69**, 020101(R) (2004).
[19] S. Pillet *et al.*, Phys. Rev. B **74**, 140101(R) (2006).
[20] See EPAPS Document No. E-PRLTAO-103-067930 for methods and additional data. For more information on EPAPS, see http://www.aip.org/pubservs/epaps.html.
[21] E. Collet *et al.*, Acta Crystallogr. Sect. B (to be published).
[22] S. Floquet *et al.*, Dalton Trans. **9**, 1734 (2005).
[23] W. Gawelda *et al.*, Phys. Rev. Lett. **98**, 057401 (2007).
[24] A. J. Simaan *et al.*, Chem. Eur. J. **11**, 1779 (2005).
[25] The different values of X_{HS} in Figs. 3(a) and 4(a) result from different excitation densities used in the corresponding experiments.
[26] Ch. Bressler *et al.*, Science **323**, 489 (2009).
[27] M. Khalil *et al.*, J. Phys. Chem. A **110**, 38 (2006).
[28] N. Moisan *et al.*, C. R. Chimie **11**, 1235 (2008).
[29] D. Fritz *et al.*, Science **315**, 633 (2007).
[30] K. Ishida and K. Nasu, Phys. Rev. Lett. **100**, 116403 (2008).